Journal of Earthquake Engineering
Vol. 10, Special Issue 1 (2006) 1–30

Imperial College Press
www.icpress.co.uk

AN ISOGEOMETRIC ANALYSIS APPROACH FOR THE STUDY OF STRUCTURAL VIBRATIONS

A. REALI*

Dipartimento di Meccanica Strutturale,
Università degli Studi di Pavia, via Ferrata 1, 27100, Pavia, Italy

and

European School for Advanced Studies in Reduction of
Seismic Risk (ROSE School), Pavia, Italy
alessandro.reali@unipv.it

The concept of Isogeometric Analysis recently introduced by Hughes *et al.* [2005] is herein applied to the study of structural vibrations. In this framework, the favourable behaviour of the method is verified and compared with some classical finite element results. Numerical experiments are shown for structural one-, two- and three-dimensional problems in order to test the performance of this promising technique in the field of the analysis of natural frequencies and modes.

Keywords: NURBS; isogeometric analysis; structural vibrations; discrete spectrum; finite element analysis; rotation-free bending elements; weak boundary conditions.

1. Introduction

Recently proposed by Hughes *et al.* [2005], Isogeometric Analysis consists of an isoparametric analysis approach where basis functions generated from Non-Uniform Rational B-Splines (commonly referred to as NURBS) are employed in order to describe both the geometry and the unknown variables of the problem. Its name ("isogeometric") is due to the fact that the use of NURBS leads to an exact geometric description of the domain, while in standard finite element analysis it is necessarily approximated by means of a mesh. It is to be noted that, as NURBS are the standard functions for describing and modelling objects in computer aided design (CAD), the term "exact" should be read in this context as "as exact as CAD modelling can be" (see Piegl and Tiller [1997] and Rogers [2001]).

The fact that even the coarsest mesh retains exact geometry makes a direct refinement possible without any need of going back to the CAD model from which the mesh has been generated; finite element analysis, instead, needs to interact with the CAD system at every refinement step, except in the case of very simple geometries.

*Tel.: +39-0382-985475, Fax: +39-0382-528422.

Moreover, besides the equivalents of classical finite element h- and p-refinements, another higher-continuity refinement strategy, named k-refinement, is possible.

Among the many advantages arising from this NURBS-based approach and highlighted in Hughes *et al.* [2005], some properties such as the high-order continuity of the bases and the consistent mass matrix point-wise positivity seem particularly suitable and promising for frequency analysis. So, the goal of this paper is to investigate the behaviour of this new method when applied to the study of structural vibration problems.

The organization of this article is as follows:
Section 2 is devoted to a brief introduction to NURBS and Isogemetric Analysis. Then the application of the method to the analysis of structural vibrations is presented through different structural examples. In particular, Sec. 3 deals with one-dimensional problems (i.e. rods and beams) and Sec. 4 with two-dimensional problems (i.e. membranes and plates). The good results of this approach for all of these case studies are shown and for 1D problems its superior behaviour with respect to classical finite element schemes is revealed. In Sec. 5, a three-dimensional circular problem is considered and solved. In this example the property of the method of capturing exact geometry with coarse meshes is also exploited. The last section draws conclusions and proposes some future development for research in the field of Isogeometric Analysis for structural dynamics.

Finally, it is to be stressed that, in general, Isogeometric Analysis approaches not based on Non-Uniform Rational B-Splines can be constructed as well. However, as NURBS are the most widespread functions in CAD technology, in this study only a NURBS-based version of Isogeometric Analysis is considered.

2. NURBS and Isogeometric Analysis

Non-Uniform Rational B-Splines are the standard way of describing and constructing curves and surfaces in the fields of CAD and computer graphics, so these functions are widely described in the related literature (refer for instance to Piegl and Tiller [1997], Rogers [2001], and references therein). The aim of this section is to introduce them briefly and to present the main guidelines of Isogeometric Analysis. The interested reader may refer to Hughes *et al.* [2005] for a detailed presentation of this new analysis approach.

2.1. *B-Splines*

B-Splines are piece-wise polynomial curves whose components are defined as the linear combination of B-Spline basis functions and the components of some points in the space, referred to as *control points*. Fixed the *order* of the B-Spline (i.e. the degree of polynomials), to construct the basis functions the so-called *knot vector* needs to be introduced, as it is a fundamental ingredient for this operation.

2.1.1. *Knot vectors*

A *knot vector* Ξ is a set of non-decreasing real numbers which constitutes a set of coordinates for the parametric space of the curve:

$$\Xi = [\xi_1, \ldots, \xi_{n+p+1}],$$

p being the B-Spline order and n the number of basis functions and control points needed for the description of the curve. A knot vector is *uniform* if its knots are equally spaced and *non-uniform* otherwise; moreover, it is *open* if its first and last knots are repeated $p+1$ times.

In the following, only *open knot vectors* are considered. A remarkable property is that basis functions constructed from open knot vectors are interpolatory at the ends of the "patch" $[\xi_1, \xi_{n+p+1}]$, but, in general, this is not true in correspondence of interior knots.

2.1.2. *Basis functions*

Given a knot vector $\Xi = [\xi_1, \ldots, \xi_{n+p+1}]$, the definition of the n B-Spline basis functions of order p is given recursively as follows.

For $p = 0$ (i.e. piece-wise constant basis functions):

$$N_{i,0}(\xi) = \begin{cases} 1 & \text{if } \xi_i \leq \xi < \xi_{i+1} \\ 0 & \text{otherwise;} \end{cases} \tag{1}$$

for $p \geq 1$:

$$N_{i,p}(\xi) = \frac{\xi - \xi_i}{\xi_{i+p} - \xi_i} N_{i,p-1}(\xi) + \frac{\xi_{i+p+1} - \xi}{\xi_{i+p+1} - \xi_{i+1}} N_{i+1,p-1}(\xi). \tag{2}$$

As an example, in Fig. 1 the $n = 9$ cubic basis functions generated from the open knot vector $\Xi = [0, 0, 0, 0, 1/6, 1/3, 1/2, 2/3, 5/6, 1, 1, 1, 1]$ are reported.

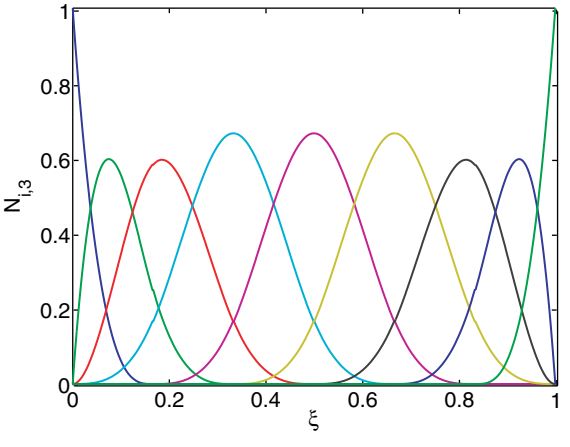

Fig. 1. Cubic basis functions from an open knot vector.

An important property of these functions is that they are C^{p-1}-continuous when there are no repeated internal knots. In fact, a multiplicity of k for a knot implies that the function is C^{p-k}-continuous at that location. Accordingly, if a knot has a multiplicity of p, the basis function is C^0 and interpolatory in correspondence of that knot.

Other remarkable properties are that B-Spline basis functions from open knot vectors constitute partitions of unity (i.e. $\sum_{i=1}^{n} N_{i,p}(\xi) = 1 \ \forall \xi$), the support of the ith basis function of order p is compact and contained in the interval $[\xi_i, \xi_{i+p+1}]$, and, finally, B-Spline basis functions are non-negative (i.e. $N_{i,p} \geq 0 \ \forall \xi$).

2.1.3. *B-Spline curves*

As a consequence of what was seen above, given the order p of a B-Spline and a knot vector, n basis functions are defined. Now, given n points in $\mathbb{R}^d$, referred to as *control points*, the components of the piece-wise polynomial B-Spline curve $\mathbf{C}(\xi)$ of order p can be obtained by taking the linear combination of the basis functions weighted by the components of the control points:

$$\mathbf{C}(\xi) = \sum_{i=1}^{n} N_{i,p}(\xi)\mathbf{B}_i, \tag{3}$$

with $\mathbf{B}_i$ being the ith control point.

The piece-wise linear interpolation of the control points is called *control polygon*. In Fig. 2, a cubic 2D B-Spline curve generated with the basis functions shown in Fig. 1 is reported together with its control polygon.

It is important to stress that a B-Spline curve has continuous derivatives of order $p-1$, which can be decreased by k if a knot or a control point has multiplicity of $k+1$.

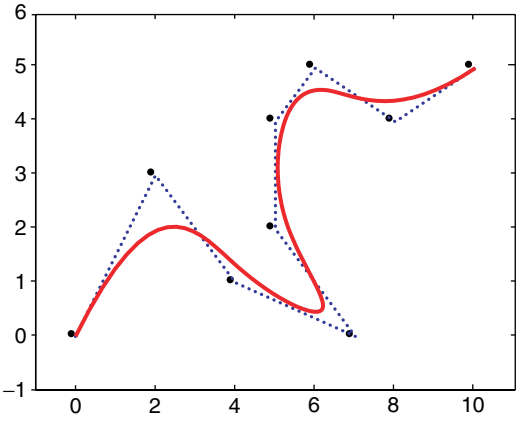

Fig. 2. Piece-wise cubic B-Spline curve (solid line) and its control polygon (dotted).

Moreover, an important property of these curves is the so-called *affine covariance*, i.e. applying an affine transformation only to the control points of a curve, the transformation of the whole curve is obtained.

2.1.4. *B-Spline solids*

By means of tensor products, B-Spline surfaces and solids can be constructed as well. Given a net of $n \times m \times l$ control points $\mathbf{B}_{i,j,k}$ (*control net*) and three knot vectors:

$$\Xi = [\xi_1, \ldots, \xi_{n+p+1}], \quad \mathrm{H} = [\eta_1, \ldots, \eta_{m+q+1}] \quad \text{and} \quad \mathrm{Z} = [\zeta_1, \ldots, \zeta_{l+r+1}],$$

the 1D basis functions $N_{i,p}$, $M_{j,q}$ and $L_{k,r}$ (with $i = 1, \ldots, n$, $j = 1, \ldots, m$ and $k = 1, \ldots, l$), of order p, q and r respectively, can be constructed. The B-Spline solid is then:

$$\mathbf{S}(\xi, \eta, \zeta) = \sum_{i=1}^{n} \sum_{j=1}^{m} \sum_{k=1}^{l} N_{i,p}(\xi) M_{j,q}(\eta) L_{k,l}(\zeta) \mathbf{B}_{i,j,k}. \tag{4}$$

2.2. *Non-uniform rational B-Splines*

A rational B-Spline in $\mathbb{R}^d$ is the projection onto the d-dimensional physical space of a non-rational (i.e. polynomial) B-Spline defined in the $(d+1)$-dimensional homogeneous coordinate space. The interested reader may find a complete discussion of these space projections in Rogers [2001] and in the references therein.

By means of this technique, a number of geometric entities are obtained and, in particular, all the conic sections are constructed exactly. The projective transformation of a B-Spline curve yields a *rational polynomial* (i.e. an expression obtained from the ratio of polynomials) and this is the reason for the name "rational" B-Splines.

Starting from a set $\mathbf{B}_i^w$ $(i = 1, \ldots, n)$ of control points ("projective points") for a B-Spline curve in $\mathbb{R}^{d+1}$ with knot vector Ξ, the control points for the NURBS curve in $\mathbb{R}^d$ are obtained as:

$$(\mathbf{B}_i)_j = \frac{(\mathbf{B}_i^w)_j}{(\mathbf{B}_i^w)_{d+1}}, \quad j = 1, \ldots, d, \tag{5}$$

where $(\mathbf{B}_i)_j$ is the jth component of the vector $\mathbf{B}_i$ and $w_i = (\mathbf{B}_i^w)_{d+1}$ the ith *weight*.

Then, the NURBS basis functions of order p (i.e. derived from B-Spline basis functions of order p) are:

$$R_i^p(\xi) = \frac{N_{i,p}(\xi) w_i}{\sum_{\hat{i}=1}^{n} N_{\hat{i},p}(\xi) w_{\hat{i}}}, \tag{6}$$

and the NURBS curve components are the linear combination of the basis functions weighted by the components of control points, that is:

$$\mathbf{C}(\xi) = \sum_{i=1}^{n} R_i^p(\xi) \mathbf{B}_i. \tag{7}$$

Rational surfaces and solids are defined in terms of B-Spline basis functions in an analogous way. Accordingly, the basis functions for a solid NURBS are:

$$R^{p,q,r}_{i,j,k}(\xi,\eta,\zeta) = \frac{N_{i,p}(\xi)M_{j,q}(\eta)L_{k,r}(\zeta)w_{i,j,k}}{\sum_{\hat{i}=1}^{n}\sum_{\hat{i}=1}^{m}\sum_{\hat{k}=1}^{l} N_{\hat{i},p}(\xi)M_{\hat{j},q}(\eta)L_{\hat{k},r}(\zeta)w_{\hat{i},\hat{j},\hat{k}}}. \tag{8}$$

As a result NURBS surfaces and solids can be seen as the projective transformations of tensor product piece-wise polynomial entities.

It is to be noted that NURBS are a generalisation of B-Splines, as it is possible to obtain B-Splines from NURBS by simply taking all weights equal. Moreover, NURBS enjoy the properties of affine covariance and of having basis functions from open knot vectors which form partitions of unity $\left(\text{i.e. } \sum_{i=1}^{n} R_i^p(\xi) = 1 \ \forall \xi\right)$ and with the same continuity properties and supports as B-Spline basis functions.

2.3. *Isogeometric analysis*

Hughes *et al.* [2005] propose the concept of *Isogeometric Analysis* as an exact geometry alternative to standard finite element analysis. The main guidelines for such a technique are summarised in the following:

- A mesh for a NURBS patch is defined by the product of open knot vectors; for instance, a 3D mesh is given by $\Xi \times \mathrm{H} \times \mathrm{Z}$.
- The domain is subdivided into "elements" by knot spans.
- The support of each basis function is made up of a small number of elements.
- The geometry is defined by the control points associated to the basis functions.
- The isoparametric concept is invoked, i.e. the unknown variables are represented in terms of the same basis functions defining geometry; their coefficients are the degrees-of-freedom, referred to as *control variables*.
- The arrays constructed from isoparametric NURBS patches can be assembled into global arrays in the same way as with finite elements (cf. Hughes [2000], Chapter 2).
- Dirichlet boundary conditions are applied to the control variables, while Neumann boundary conditions are satisfied naturally as it happens with standard finite element formulations (cf. Hughes [2000], Chapters 1 and 2).

Finally, it is important to highlight that, when applied to structural analysis (which is the field of interest of the present work), isoparametric NURBS patches represent exactly all rigid body motion and constant strain states. So structures assembled from compatible NURBS patches pass standard "patch tests" (see Hughes [2000], Chapters 3 and 4).

3. Structural Vibrations of 1D Problems

In this section two types of 1D structural problems are analysed by means of Isogeometric Analysis. They are, respectively, the solution of the generalised eigenvalue problems arising from the 1D Laplace equation (i.e. the structural vibrations

of a rod) and from the 1D biharmonic equation (i.e. the structural vibrations of an Euler-Bernoulli beam). Even if in 1D problems no advantage is taken from the exact geometry capabilities of the formulation (in fact, due to geometric simplicity, all weights are equal to 1 and NURBS collapse to B-Splines), the high continuity and point-wise non-negativity of the basis functions (implying element-wise positivity of the consistent mass matrix) lead anyway to the good results shown in the following.

3.1. *Elastic rod longitudinal vibrations*

The first investigated problem consists of the study of the natural structural vibrations for an elastic fixed-fixed rod of unit length, whose natural frequencies and modes, assuming unit material parameters, are governed by (refer to Hughes [2000], Chapter 7, for details about the formulation):

$$\begin{aligned} u_{,xx} + \omega^2 u = 0 \quad \text{for } x \in]0,1[\\ u(0) = u(1) = 0. \end{aligned} \tag{9}$$

In terms of natural frequencies, the exact solution of problem (9) is:

$$\omega_n = n\pi, \quad \text{with } n = 1, 2, 3 \ldots . \tag{10}$$

After writing the weak formulation for (9) and performing the discretisation of the domain (cf. Hughes [2000], Clough and Penzien [1993] and Chopra [2001]), a generalised eigenproblem of the following form is easily obtained:

$$\mathbf{K} - \omega_n^2 \mathbf{M} = \mathbf{0}, \tag{11}$$

where $\mathbf{K}$ and $\mathbf{M}$ are respectively the stiffness and the mass matrix associated to the formulation.

3.1.1. *Numerical experiments*

The first numerical experiment concentrates on solving the generalised eigenproblem (11) with both finite elements and Isogeometric Analysis using quadratic basis functions (note that for linear approximation both the approaches have exactly the same basis functions, the so-called "hat functions"). The obtained natural frequencies ω_n^h are reported in Fig. 3. They are normalised with respect to the exact solution (10) and plotted versus the number of modes n, normalised with respect to the total number of degrees-of-freedom N. To produce the spectra of Fig. 3, for both the formulations a number of degrees-of-freedom $N = 999$ have been employed, but the results are anyway invariant with respect to N.

Figure 3 points out the superior behaviour of the NURBS-based approach as compared with finite elements, which show a bad second half of the discrete spectrum. This first result confirms the effectiveness of the idea of employing this new technique for structural vibration problems.

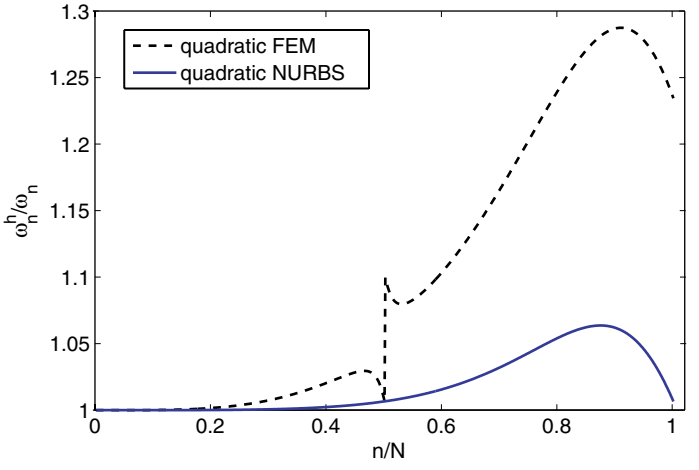

Fig. 3. Rod problem: normalised discrete spectra using quadratic finite elements and NURBS.

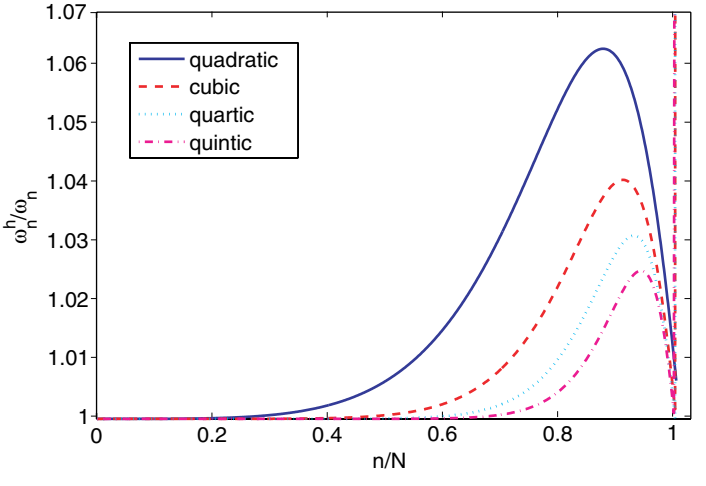

Fig. 4. Rod problem: normalised discrete spectra using different order NURBS basis functions.

Then, the same eigenvalue analysis has been carried out using higher-order NURBS basis functions. The resulting discrete spectra are presented in Fig. 4; the analyses have been performed using $N = 1000$ control points.

Increasing the order p of the basis functions, the results show higher order of accuracy ($2p$, while standard finite elements achieve $p + 1$; see Reali [2004] for the computation of the order of accuracy using quadratic and cubic NURBS) and decreasing errors. Anyway, increasing p also produces the appearance of strange

frequencies at the very end of the spectrum, referred to in the following as "outlier frequencies" (in analogy with outlier values in statistics, refer for instance to Montgomery *et al.* [2003]), whose number and error increase with p. These outliers constitute a discrete "optical branch" of the spectrum (similar to the "bad part" of the finite element spectrum observed in Fig. 3) and can be ignored in vibration analysis. Their participation can be damped out in transient response by means of implicit time integration algorithms as shown in Hilber *et al.* [1977]; they could however be a problem in explicit transient analysis because they would lead to too small time steps to guarantee stability, but it will be shown later how to completely avoid their appearance.

Moreover, Fig. 5 shows a plot of the average relative error over the whole spectrum $\left(\frac{\sum_{n=1}^{N}(\omega_n^h-\omega_n)/\omega_n}{N}\right)$ versus the order p, as compared with the one obtained excluding outlier frequencies from the average ($N = 1000$ control points have been employed).

Finally, Figs. 6–8 show that the order of convergence for frequencies computed using NURBS is $O(h^{2p})$, as with finite elements.

3.1.2. *Discrete spectrum analytical determination*

Following the derivations of Hughes [2000], Chapter 9, the discrete spectra, previously determined numerically, can be computed also analytically.

The starting point for this operation is the determination of the mass and stiffness matrices for a generic interior element (notice that for interior elements the

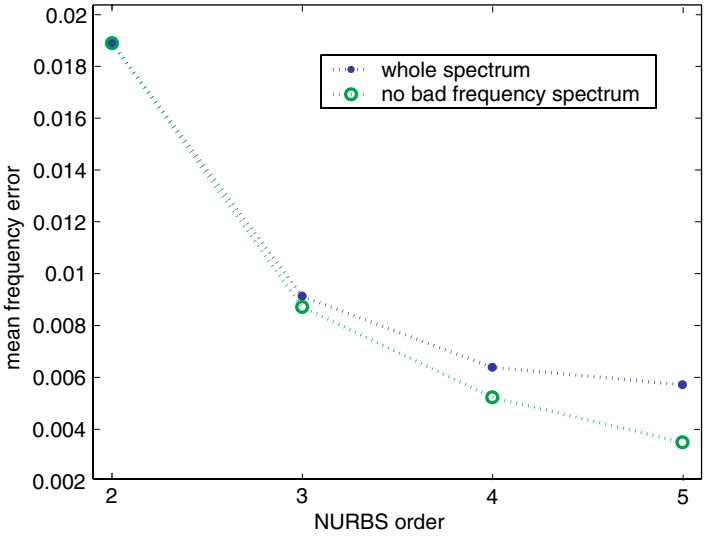

Fig. 5. Rod problem: average relative error over the whole spectrum (dots) and excluding outlier frequencies (circles).

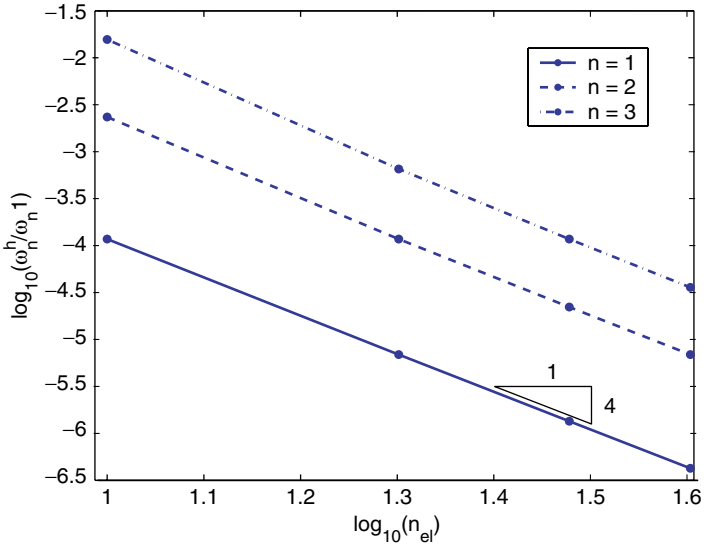

Fig. 6. Rod problem: order of convergence for the first three frequencies using quadratic NURBS.

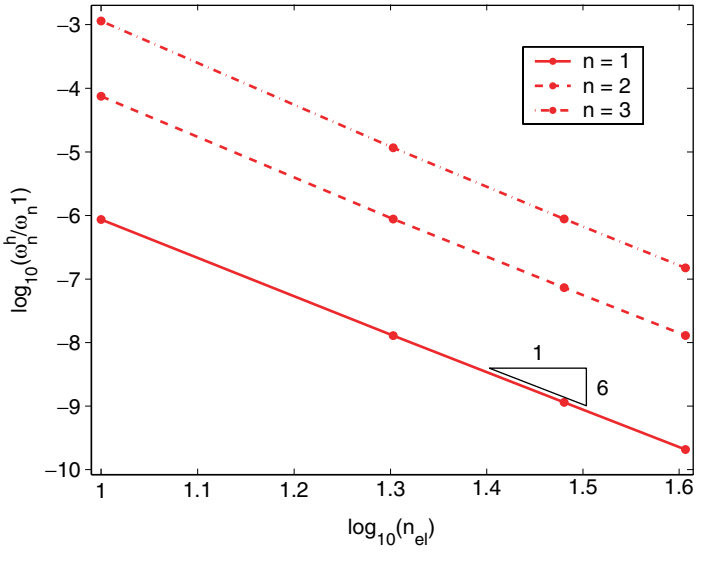

Fig. 7. Rod problem: order of convergence for the first three frequencies using cubic NURBS.

basis functions are all the same, see Fig. 1 as an example, and so the element matrices). Using quadratic NURBS they are respectively:

$$\mathbf{M}^e = \frac{h}{120}\begin{bmatrix} 6 & 13 & 1 \\ 13 & 54 & 13 \\ 1 & 13 & 6 \end{bmatrix} \quad \text{and} \quad \mathbf{K}^e = \frac{1}{6h}\begin{bmatrix} 2 & -1 & -1 \\ -1 & 2 & -1 \\ -1 & -1 & 2 \end{bmatrix}, \tag{12}$$

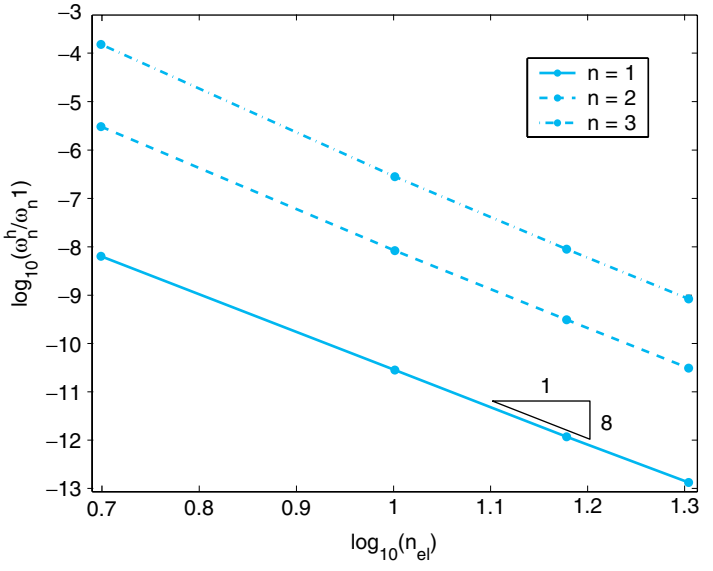

Fig. 8. Rod problem: order of convergence for the first three frequencies using quartic NURBS.

with $h = 1/n_{el} = 1/(n_{cp} - p)$ (n_{el} is the number of elements, n_{cp} the total number of control points and $p = 2$ is the order of the basis functions). Given $\mathbf{M}^e$ and $\mathbf{K}^e$, the scalar equation of motion for the generic interior control point A can be written as:

$$\begin{aligned} &\frac{h}{120}(\ddot{u}_{A-2} + 26\ddot{u}_{A-1} + 66\ddot{u}_A + 26\ddot{u}_{A+1} + \ddot{u}_{A+2}) + \\ &\quad -\frac{1}{6h}(u_{A-2} + 2u_{A-1} - 6u_A + 2u_{A+1} + u_{A+2}) = 0. \end{aligned} \tag{13}$$

For compactness, Eq. (13) can be rewritten as:

$$\frac{h^2}{20}\alpha\ddot{u}_A - \beta u_A = 0, \tag{14}$$

where α and β are operators acting as follows:

$$\begin{aligned} \alpha x_i &= x_{i-2} + 26x_{i-1} + 66x_i + 26x_{i+1} + x_{i+2}, \\ \beta x_i &= x_{i-2} + 2x_{i-1} - 6x_i + 2x_{i+1} + x_{i+2}. \end{aligned} \tag{15}$$

Separating variables as:

$$u_A(t) = \phi_A q(t), \tag{16}$$

and substituting this expression into Eq. (14), after adding and subtracting $\frac{(\omega^h h)^2}{20}\alpha u_i$, it is possible to obtain:

$$(\ddot{q} + (\omega^h)^2 q)\frac{h^2}{20}\alpha\phi_A - \left(\frac{(\omega^h h)^2}{20}\alpha\phi_A + \beta\phi_A\right) q = 0, \tag{17}$$

whose satisfaction is achieved by selecting ϕ_A and q such that:

$$\left(\frac{(\omega^h h)^2}{20}\alpha + \beta\right)\phi_A = 0, \tag{18}$$

and

$$\ddot{q} + (\omega^h)^2 q = 0. \tag{19}$$

Assuming a solution (valid for fixed-fixed boundary conditions) for Eq. (18) of the form:

$$\phi_A = C\sin(A\omega h), \quad \text{with } \omega = n\pi, \tag{20}$$

it is possible to rewrite Eq. (18) as:

$$\left(\frac{(\omega^h h)^2}{20}\alpha + \beta\right)\sin(A\omega h) = 0. \tag{21}$$

Now, substituting expressions (15) for α and β operators, by means of the trigonometric identity $\sin(a \pm b) = \sin(a)\cos(b) \pm \sin(b)\cos(a)$ the following is obtained:

$$\frac{(\omega^h h)^2}{20}(16 + 13\cos(\omega h) + \cos^2(\omega h)) - (2 - \cos(\omega h) - \cos^2(\omega h)) = 0, \tag{22}$$

which can be solved for $\frac{\omega^h}{\omega}$, yielding:

$$\frac{\omega^h}{\omega} = \frac{1}{\omega h}\sqrt{\frac{20(2 - \cos(\omega h) - \cos^2(\omega h))}{16 + 13\cos(\omega h) + \cos^2(\omega h)}}. \tag{23}$$

Equation (23) is the analytical expression for the normalised discrete spectrum for the problem under investigation, computed using quadratic NURBS basis functions. Analogous calculations can be carried out also for higher order approximations. In Fig. 9 analytical and numerical discrete spectra for quadratic and cubic approximations are reported; to obtain the numerical discrete spectra, 2000 control points have been employed. It is to be noted that the only differences are in the outlier frequencies at the end of the cubic NURBS discrete spectrum. The analytical expression for the discrete spectrum, obtained using cubic NURBS, is:

$$\frac{\omega^h}{\omega} = \frac{1}{\omega h}\sqrt{\frac{42(16 - 3\cos(\omega h) - 12\cos^2(\omega h) - \cos^3(\omega h))}{272 + 297\cos(\omega h) + 60\cos^2(\omega h) + \cos^3(\omega h)}}, \tag{24}$$

and has been computed with the same procedure detailed for the quadratic case.

Remark 1

All the numerical results shown up to now have been obtained using control points computed, starting from the knot vector, with the procedure proposed by Hughes *et al.* [2005]. In this way a linear parametrisation (i.e. constant Jacobian) is obtained. As seen, the obtained results are very good, except for the presence at the end of the discrete spectrum of outlier frequencies, which get worse for higher order

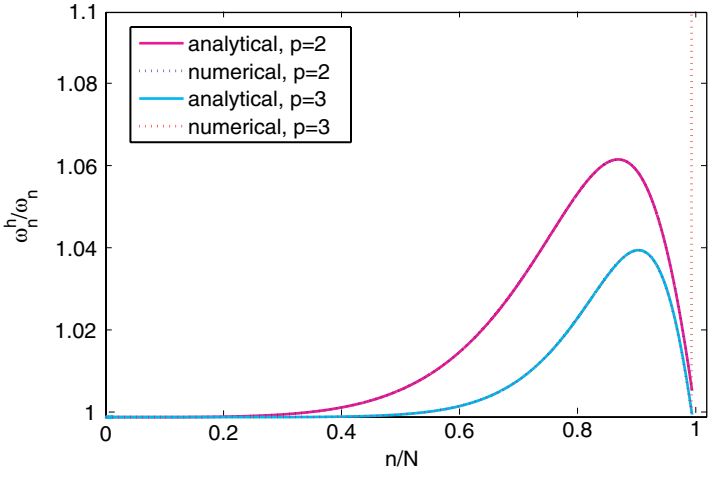

Fig. 9. Rod problem: analytical versus numerical discrete spectrum computed using quadratic and cubic NURBS.

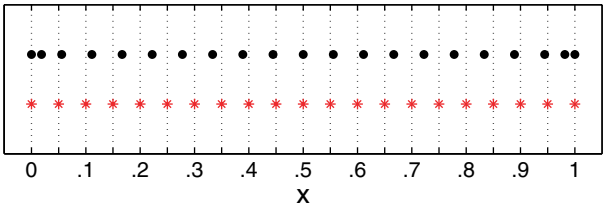

Fig. 10. Distribution of control points for linear parametrisation (dots) as compared with equally spaced control points (asterisks) (cubic NURBS, 21 control points).

approximations. A way to avoid this behaviour is to employ equally spaced control points (in Fig. 10 it is possible to see the difference between the distribution of 21 control points in the case of linear parametrisation and of equally spaced points using cubic NURBS), even if this choice corresponds to a nonlinear parametrisation (see Figs. 11 and 12 for a plot of the parametrisation $x(\xi)$ and of its Jacobian $J(\xi) = \frac{\mathrm{d}x(\xi)}{\mathrm{d}\xi}$ for the cases of linear parametrisation and of equally spaced control points of Fig. 10).

Finally, Fig. 13 reports the discrete spectra computed using equally spaced control points: they do not show any outlier and they perfectly coincide with those computed analytically (and shown in Fig. 9 for quadratic and cubic NURBS).

In order to find an explanation for the presence of outlier frequencies and for the cure to this pathology proposed above, it is necessary to get back to the discrete spectrum obtained using quadratic finite elements and reported in Fig. 3. In that case, two different solution branches are present in the spectrum, due to the fact that there exist two different equations associated to the problem and half of the total equations are of one type and half of the other. The same is also true for

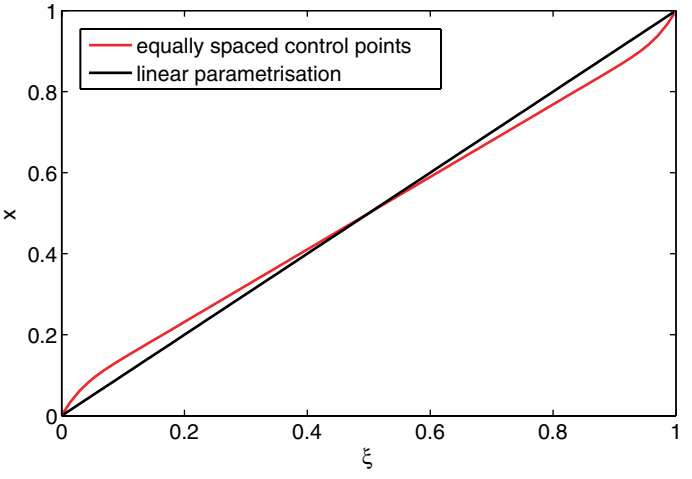

Fig. 11. Plot of the parametrisation for the cases of equally spaced control points and of linear parametrisation (cubic NURBS, 21 control points).

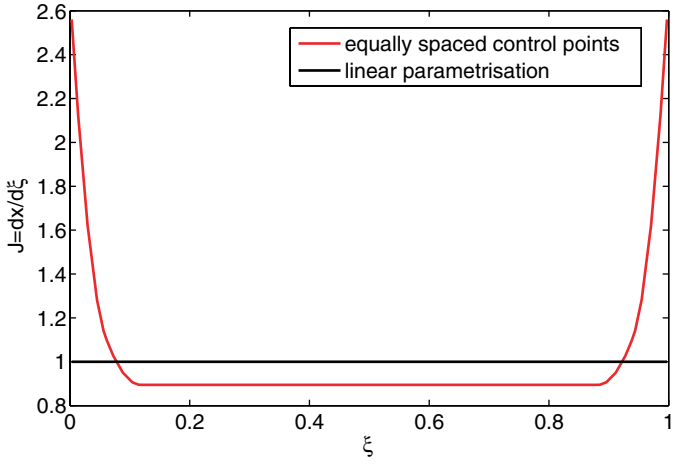

Fig. 12. Plot of the Jacobian of the parametrisation for the cases of equally spaced control points and of linear parametrisation (cubic NURBS, 21 control points).

Isogeometric Analysis, but here only few equations (those associated to control points close to the boundary) are different from the others, giving rise to a small number of outlier frequencies. The choice of equally spaced control points makes all the equations equal, avoiding the presence of outliers.

However, more research still needs to be carried out on this topic, and it will be the object of future investigations.

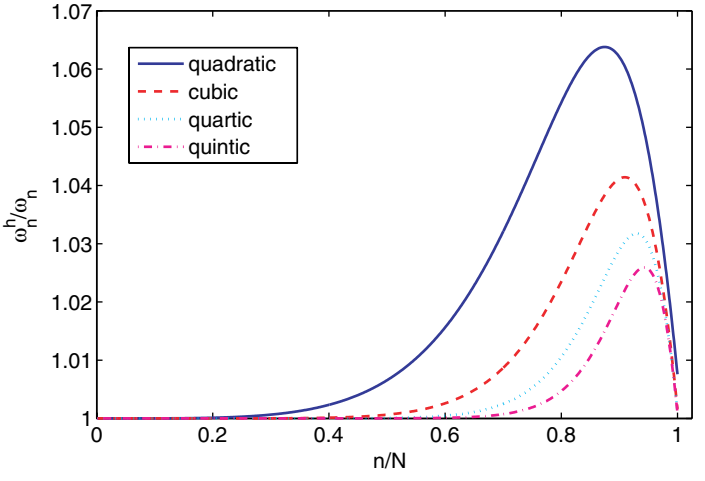

Fig. 13. Rod problem: normalised discrete spectra using equally spaced control points.

Remark 2

This paper deals with consistent mass theory, also because it should be more suitable than lumped mass when high order approximations are involved. Anyway, some preliminary tests using lumped mass have been performed, too. In Reali [2004] it is shown that the classical lumped mass formulation that works well with finite elements, does not work in this context. The order of accuracy does not increase with the order p (only second order accuracy is achieved in each case), while errors increase. However, a higher order of accuracy and better results may be obtained employing some special non-uniform knot vector and quadrature scheme choices, in a fashion similar to what is done in Fried and Malkus [1976].

It can then be concluded that, about the topic of lumped mass techniques in the framework of Isogeometric Analysis, extensive research still needs to be carried out.

3.2. *Euler-Bernoulli beam transversal vibrations*

Another interesting 1D problem is the study of the natural structural transversal vibrations of a simply-supported, unit length Euler-Bernoulli beam (refer to Hughes [2000], Chapter 7, for details about the formulation). In this case, natural frequencies and modes are governed by the following equations (assuming unit material parameters):

$$\begin{aligned} &u_{,xxxx} - \omega^2 u = 0 \quad \text{for } x \in]0,1[\\ &u(0) = u(1) = u_{,xx}(0) = u_{,xx}(1) = 0, \end{aligned} \tag{25}$$

and the exact solution, in terms of natural frequencies, is:

$$\omega_n = (n\pi)^2, \quad \text{with } n = 1, 2, 3 \ldots . \tag{26}$$

Again, after writing the weak formulation and performing the discretisation, a problem of the form of (11) is obtained.

3.2.1. *Numerical experiments*

Numerical experiments, and results as well, for the beam problem are analogous to those shown for the rod. However, before discussing them, it is necessary to remark that, while with finite elements, to solve problem (25), a classical two-node cubic Hermite beam element with two degrees-of-freedom per node (i.e. transversal displacement and rotation) is employed, the Isogeometric Analysis formulation here implemented is *rotation-free* (refer for instance to Engel *et al.* [2002]). Later in this section, also the problem of the imposition of boundary conditions on rotations will be addressed.

Figure 14 reports the discrete spectra obtained using classical cubic finite element and NURBS basis functions. It is seen that the NURBS solution behaves much better, even if two outlier frequencies are present at the end of the spectrum.

Figure 15 shows the discrete spectra obtained employing NURBS basis functions of different orders. The behaviour is similar to the one seen in the case of the rod, including outliers.

Figure 16 reports a plot of the average relative error over the whole spectrum versus the order p with the exclusion of the outlier frequencies (1000 control points have been employed).

Moreover, Figs. 17–19 show that also here the order of convergence using NURBS is the same as using finite elements, that is $O(h^{2(p-1)})$.

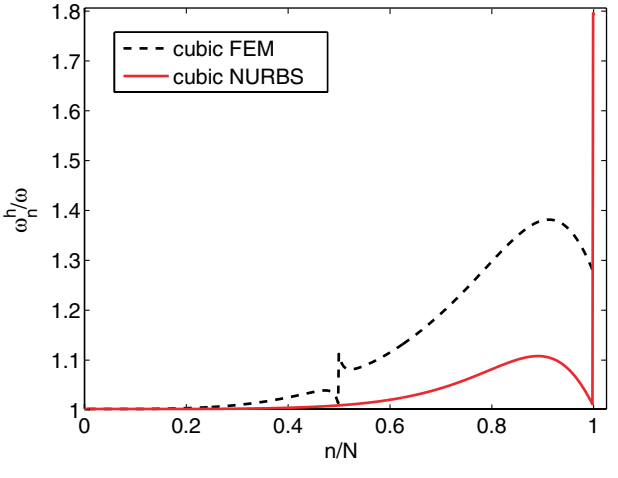

Fig. 14. Beam problem: normalised discrete spectra using cubic finite elements and NURBS.

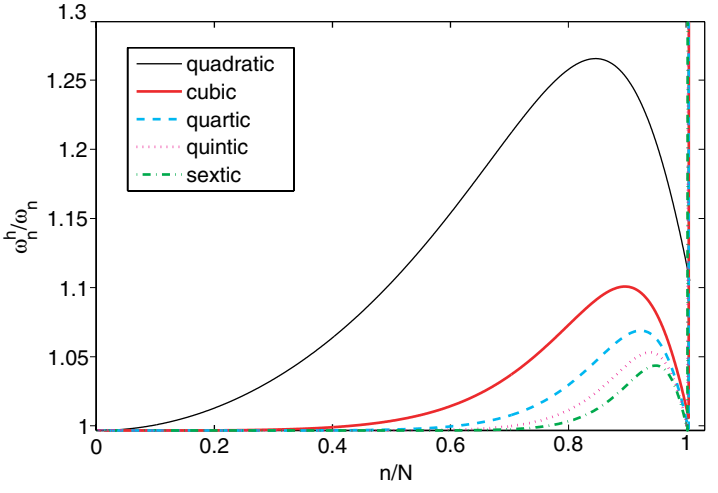

Fig. 15. Beam problem: normalised discrete spectra using different order NURBS basis functions.

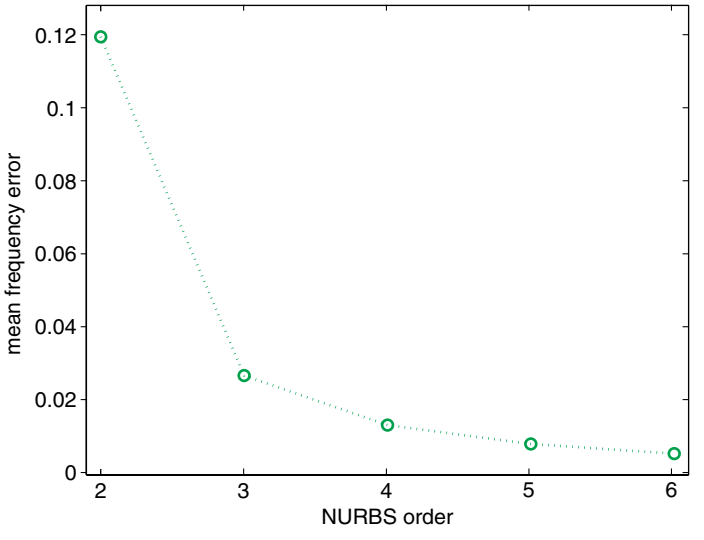

Fig. 16. Beam problem: average relative error over the spectrum with the exclusion of outlier frequencies.

The analytical computation of the discrete spectrum performed for the previous problem can be carried out in the same way as before also here. Employing cubic NURBS shape functions, for instance, the following expression is obtained:

$$\frac{\omega^h}{\omega} = \frac{1}{\omega h^2}\sqrt{\frac{210(2-3\cos(\omega h)+\cos^3(\omega h))}{272+297\cos(\omega h)+60\cos^2(\omega h)+\cos^3(\omega h)}}. \tag{27}$$

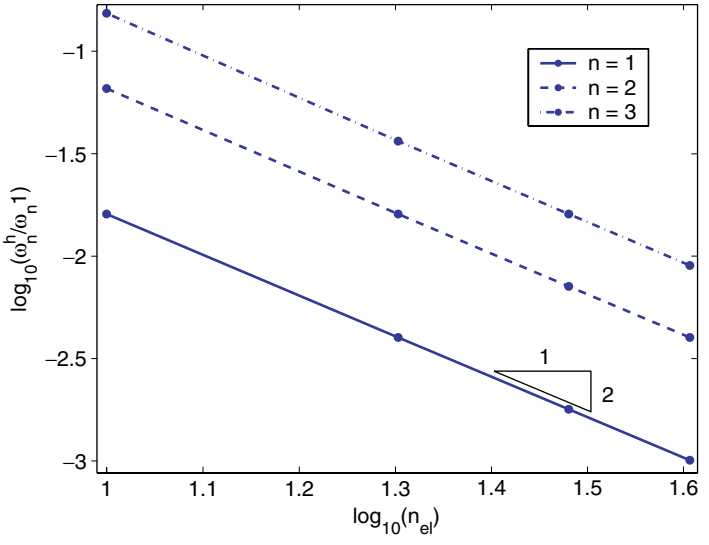

Fig. 17. Beam problem: order of convergence for the first three frequencies using quadratic NURBS.

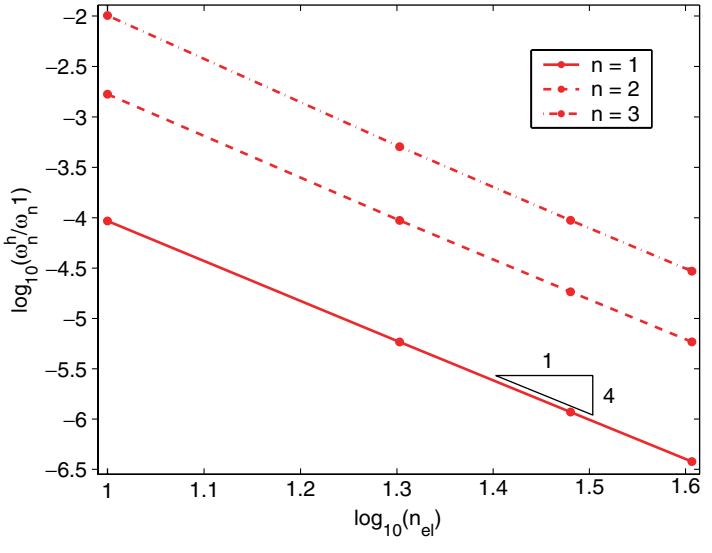

Fig. 18. Beam problem: order of convergence for the first three frequencies using cubic NURBS.

Figure 20 reports the analytical and numerical discrete spectra for cubic and quartic approximations; for numerical discrete spectrum computation 2000 control points have been employed. It is possible to see that again the only differences are in the outlier frequencies at the end of the numerical discrete spectra.

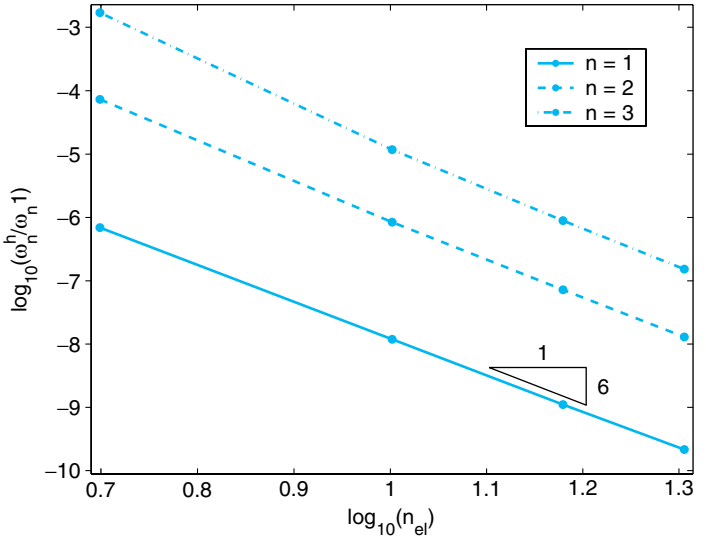

Fig. 19. Beam problem: order of convergence for the first three frequencies using quartic NURBS.

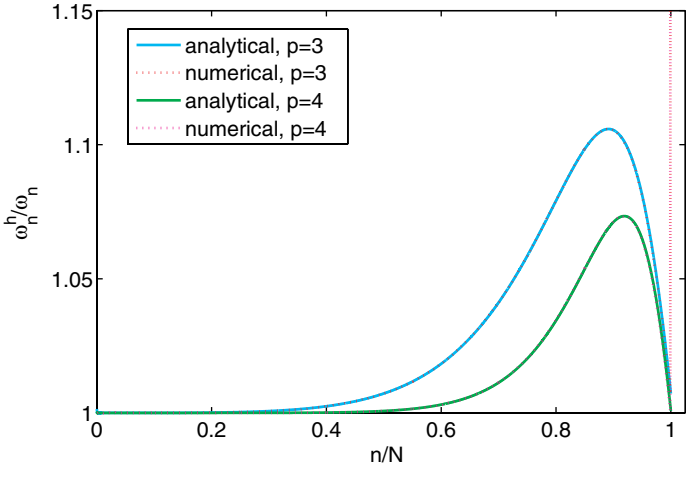

Fig. 20. Beam problem: analytical versus numerical discrete spectrum computed using cubic and quartic NURBS.

As already shown for the rod, this behaviour can be cured by means of a different choice in the distribution of the control points, i.e. using, instead of a linear parametrisation, a nonlinear one with equally spaced control points. In this way, it is possible to obtain the discrete spectra of Fig. 21, coinciding with those computed analytically and not showing any outlier.

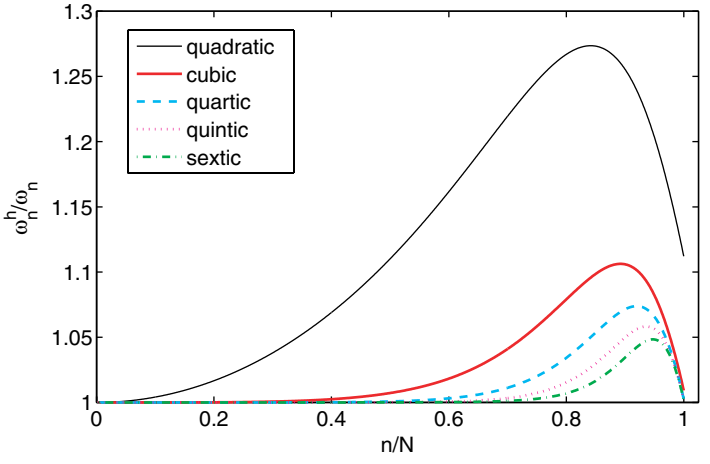

Fig. 21. Beam problem: normalised discrete spectra using equally spaced control points.

3.2.2. *Boundary conditions on rotations*

It has already been mentioned that the formulation used for the Euler-Bernoulli beam is rotation-free, i.e. the only unknowns are transversal displacements (see Engel *et al.* [2002], Oñate and Cervera [1993], Oñate and Zarate [2000], Phaal and Calladine [1992]). When needed, rotations can be computed as displacement derivatives, but they are not approximated as independent variables.

A problem that may arise is that the boundary conditions for a beam frame are usually given also on rotations. For example, in order to study the natural frequencies of one of the simplest structural member, the cantilever beam, it is necessary to solve the problem (considering unit material parameters):

$$\begin{aligned} &u_{,xxxx} - \omega^2 u = 0 \quad \text{for } x \in]0,1[\\ &u(0) = u_{,x}(0) = u_{,xx}(1) = u_{,xxx}(1) = 0, \end{aligned} \tag{28}$$

where a zero boundary condition is prescribed to the rotation of the first end ($\theta(0) = u_{,x}(0) = 0$). For this example, the following solution, reported in Chopra [2001], is taken as reference:

$$\begin{aligned} &\omega_n = \beta_n^2, \\ \text{with } \beta_1 = 1.8751, \quad &\beta_2 = 4.6941, \quad \beta_3 = 7.8548, \quad \beta_4 = 10.996 \\ \text{and} \quad &\beta_n = (n - 1/2)\pi \ \text{ for } n > 4. \end{aligned} \tag{29}$$

In order to solve this problem, two strategies are here proposed, one based on a weak boundary condition imposition and the other on the Lagrange multiplier technique.

The former approach consists of the formulation suggested in Engel *et al.* [2002], so that, in the example under investigation, the bilinear form A originating the stiffness matrix (including the weak form of the boundary condition plus a stabilisation term) is given by:

$$A(v^h, u^h) = \int_0^1 v^h_{,xx} u^h_{,xx} \mathrm{d}x + v^h_{,x} u^h_{,xx}|_{x=0} + v^h_{,xx} u^h_{,x}|_{x=0} + \tau v_{,x} u_{,x}|_{x=0}, \tag{30}$$

where v^h and u^h are the discrete test and unknown functions, respectively, and τ is a parameter of stabilisation.

In a way analogous to what is done in Prudhomme *et al.* [2001] in the framework of Poisson problems, the choice of τ can be shown to be necessarily proportional to p^2/h, where p is the order of the employed NURBS bases and $h = 1/n_{el}$ is a mesh parameter (n_{el} is the number of used elements).

By means of this formulation the cantilever beam problem (28) has been solved and the corresponding discrete spectra for NURBS of different orders are shown in Fig. 22 (1000 control points and a parameter of stabilisation $\tau = p^2/h$ have been used). It can be noticed that Fig. 22 shows the same behaviour seen for the simply-supported beam (Fig. 15).

The other way to deal with boundary conditions on rotations is the imposition of the constraint through Lagrange multipliers. With this technique the following bilinear form is obtained:

$$A(v^h, u^h) = \int_0^1 v^h_{,xx} u^h_{,xx} \mathrm{d}x + \lambda v^h_{,x}|_{x=0} + \mu u^h_{,x}|_{x=0}, \tag{31}$$

where λ is the Lagrange multiplier and μ its test counterpart.

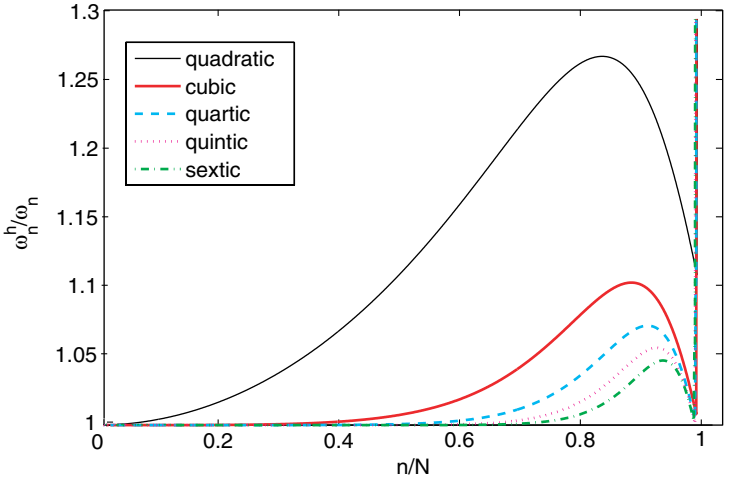

Fig. 22. Cantilever beam with weak constraint imposition: normalised discrete spectra using different order NURBS basis functions.

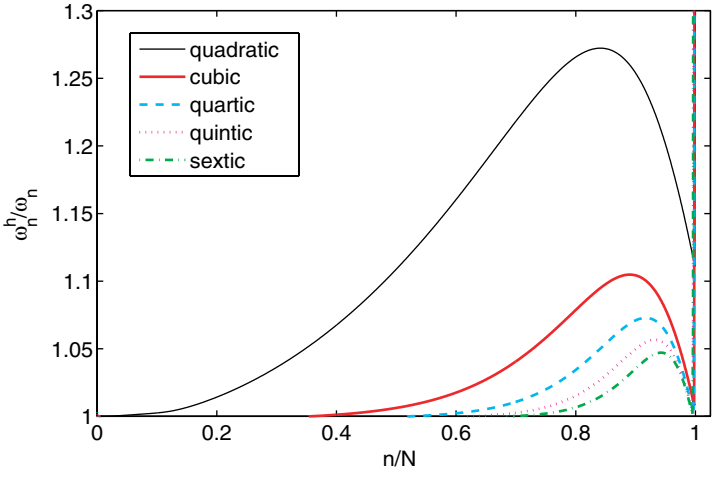

Fig. 23. Cantilever beam with Lagrange multiplier: normalised discrete spectra using different order NURBS basis functions.

This procedure has the disadvantage of introducing extra (unnecessary) variables, i.e. the multipliers, but on the other side it enforces boundary conditions on rotations exactly and needs no stabilisation. The numerical results are equivalent to those obtained from the weak approach, as shown by Fig. 23.

4. Structural Vibrations of 2D Problems

This section deals with some numerical experiments on the 2D counterparts of the rod and the Euler-Bernoulli beam problems previously illustrated, which are respectively the transversal vibrations of an elastic membrane and of a Kirchhoff plate.

4.1. *Elastic membrane transversal vibrations*

The first presented 2D problem is the study of the transversal vibrations of a square, elastic membrane fixed along its perimeter, whose natural frequencies and modes, assuming unit material parameters and edge length, are governed by the Laplace problem:

$$\begin{aligned} \nabla^2 u(x,y) + \omega^2 u(x,y) &= 0 \quad \text{for } (x,y) \in \Omega =]0,1[\times]0,1[\\ u(x,y)|_{\partial\Omega} &= 0. \end{aligned} \tag{32}$$

The exact solution in terms of natural frequencies (see for example Meirovitch [1967]) is:

$$\omega_{mn} = \pi\sqrt{m^2+n^2}, \quad \text{with } m,n = 1,2,3\ldots. \tag{33}$$

Again, a problem of the form of (11) is obtained after the discretisation of the weak formulation.

Numerical results are qualitatively analogous to those obtained for 1D problems. Figure 24 reports the normalised discrete spectra obtained employing NURBS basis functions of different order and a linear parametrisation over a 70×70 control net. Note that l is the mode number (sorted from the lowest to the highest frequency), while N is the total number of degrees-of-freedom. Also in this case the linear parametrisation leads to a bad last part of the spectrum, but, again, the presence of such a branch can be eliminated by means of an equally spaced control net as reported in Fig. 25. Finally Fig. 26 shows the average relative error over the spectra of Fig. 25.

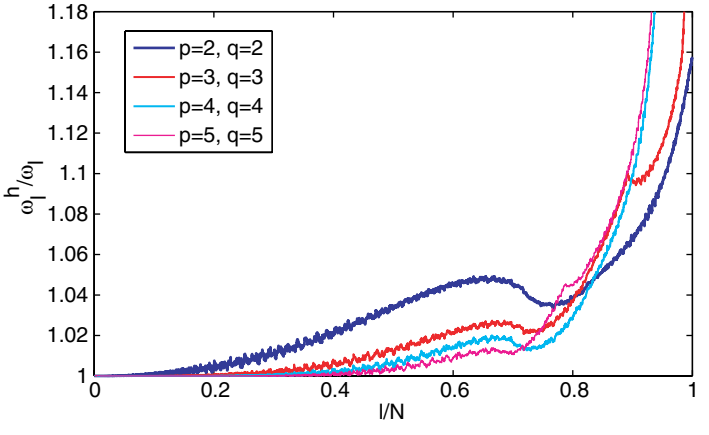

Fig. 24. Membrane problem: normalised discrete spectra using different order NURBS basis functions (70×70 control points).

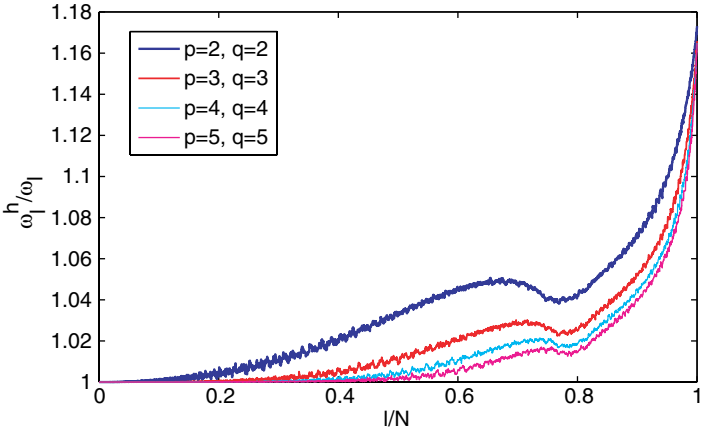

Fig. 25. Membrane problem: normalised discrete spectra using an equally spaced control net.

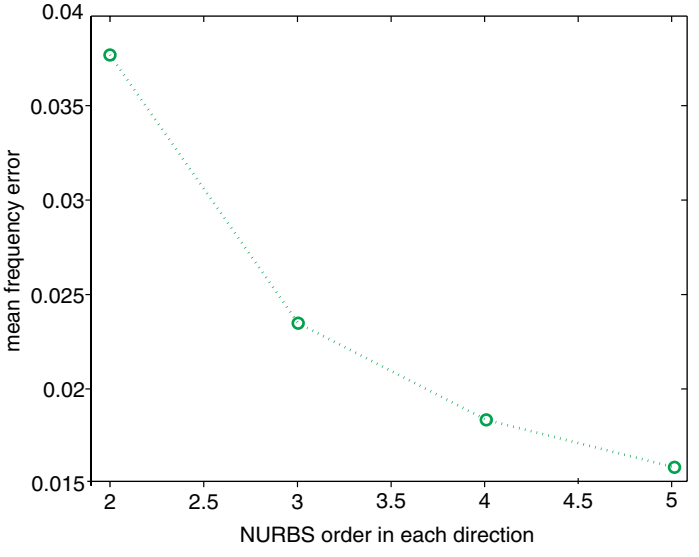

Fig. 26. Membrane problem: average relative error of the spectra shown in Fig. 25.

4.2. *Kirchhoff plate transversal vibrations*

The second studied 2D problem consists of the analysis of the transversal vibrations for a square, simply-supported Kirchhoff plate. Its natural frequencies and modes, assuming unit flexural rigidity, density and edge length, are governed by the following biharmonic problem:

$$\begin{aligned} \nabla^4 u(x,y) - \omega^2 u(x,y) = 0 \quad &\text{for } (x,y) \in \Omega =]0,1[\times]0,1[\\ u(x,y)|_{\partial\Omega} = 0, \quad & \end{aligned} \tag{34}$$

for which the exact solution (see Meirovitch [1967]) is:

$$\omega_{mn} = \pi^2(m^2 + n^2), \quad \text{with } m,n = 1,2,3\ldots. \tag{35}$$

Also for this case, a problem of the form of (11) can be obtained.

As for the Euler-Bernoulli beam, the NURBS formulation employed for this problem consists of a *rotation-free* approach. Following Engel *et al.* [2002], boundary conditions on rotations can be imposed as previously discussed for 1D cases.

Numerical results are analogous to those obtained for the elastic membrane. Figure 27 reports the normalised discrete spectra using a linear parametrisation over a 70×70 control net, while Fig. 28 shows the spectra obtained employing an equally spaced control net (i.e. no outlier frequency branches). Finally, Fig. 29 reports the average relative error computed over the spectra of Fig. 28.

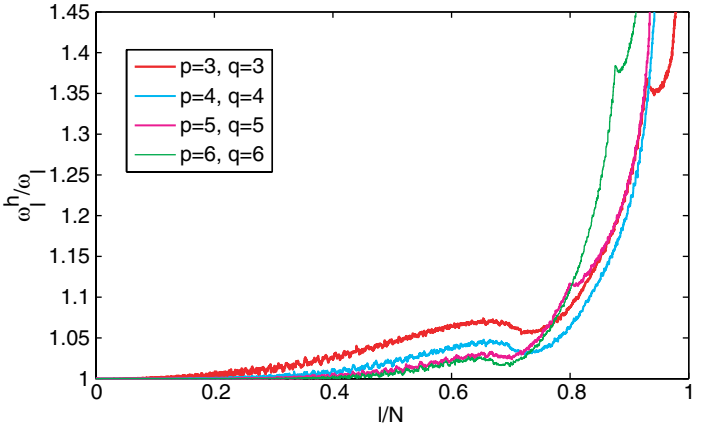

Fig. 27. Plate problem: normalised discrete spectra using different order NURBS basis functions (70×70 control points).

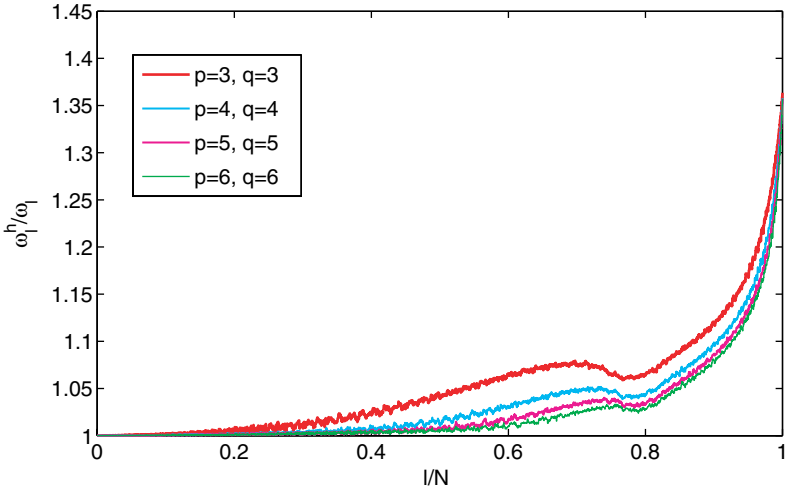

Fig. 28. Plate problem: normalised discrete spectra using an equally spaced control net.

5. Clamped Thin Circular Plate Vibrations Using 3D Solid Elements

One of the greatest advantages of Isogeometric Analysis is its capability of working with exact geometry even for coarse meshes. So, for instance, it is possible to study with few NURBS elements a circular domain without approximating it through a faceted polygon as with finite elements (e.g. a circle can be represented exactly by means of only three pieces of quadratic NURBS curves, as shown in Piegl and Tiller [1997] and Rogers [2001]).

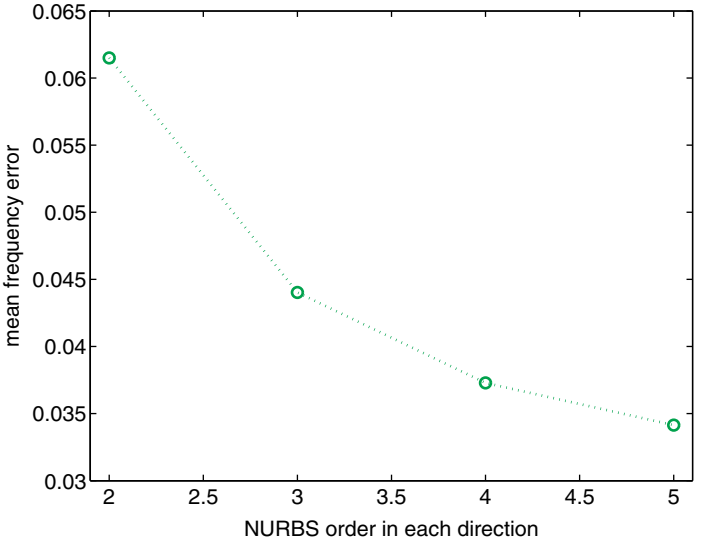

Fig. 29. Plate problem: average relative error of the spectra shown in Fig. 28.

Another important feature of this technique, addressed by Hughes *et al.* [2005], is the possibility of studying thin structures like plates and shells with 3D solid NURBS elements.

In this framework, an interesting example is the study of the vibrations of a clamped thin circular plate. The approach consists of constructing a coarse mesh (anyway capable of exactly reproducing geometry) and then elevating the order of the basis functions until a sufficient precision in the approximation of the first three frequencies is achieved. The exact solution (presented in Meirovitch [1967]) under Kirchhoff's assumptions is:

$$\omega_{mn} = C_{mn}^2 \frac{\pi^2}{R^2} \sqrt{\frac{D_E t}{\rho}} \, [rad/s], \tag{36}$$

where R is the radius of the plate, t is the thickness, $D_E = \frac{Et^3}{12(1-\nu^2)}$ is the flexural rigidity (being E and ν respectively the Young's modulus and the Poisson's ratio) and ρ is the density (mass per unit volume); for the first three frequencies the values for C_{mn} coefficients are:

$$C_{01} = 1.015, \quad C_{11} = 1.468 \quad \text{and} \quad C_{02} = 2.007.$$

The data for the problem under investigation are shown in Table 1, where concrete typical material parameters have been used. Note that the adopted radius-to-thickness ratio of 100 makes Kirchhoff's assumptions valid for this problem (i.e. it is a *thin* plate).

Table 1. Clamped circular plate: geometric and material parameters.

R	2.000	$[m]$
t	0.020	$[m]$
E	$30{\cdot}10^6$	$[KN/m^2]$
ν	0.200	[–]
ρ	2.320	$[KNs/m^4]$

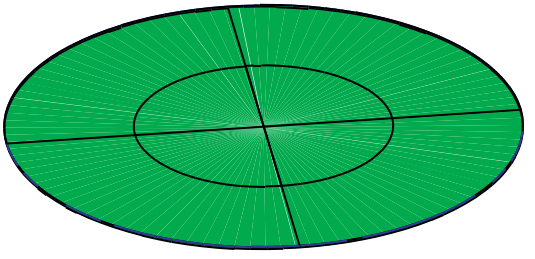

Fig. 30. Clamped circular plate: 8-element mesh.

Table 2. Clamped circular plate: numerical results as compared with the exact solution.

p	q	r	ω_{01} $[rad/s]$	ω_{11} $[rad/s]$	ω_{02} $[rad/s]$
2	2	2	138.133	1648.800	2052.440
2	3	2	56.702	267.765	276.684
3	3	2	56.051	126.684	232.788
3	4	2	54.284	124.417	212.451
4	4	2	54.284	113.209	212.451
4	5	2	54.153	112.700	210.840
Exact			53.863	112.670	210.597

The starting control net consists of $9 \times 4 \times 3$ control points and quadratic approximations in all the parametric directions are initially employed; Fig. 30 shows the corresponding mesh, which consists of a very coarse 8-element patch.

Numerical results, as compared with the exact solution, are reported in Table 2, where p, q and r are the orders of the basis functions in the circumferential, radial and vertical directions, respectively; the favourable behaviour of this kind of analysis for such a problem is revealed.

Finally, Figs. 31–33 show the shapes of the first three eigenmodes (computed using $p = 4$, $q = 5$ and $r = 2$), which are in agreement with the expected ones depicted in Meirovitch [1967].

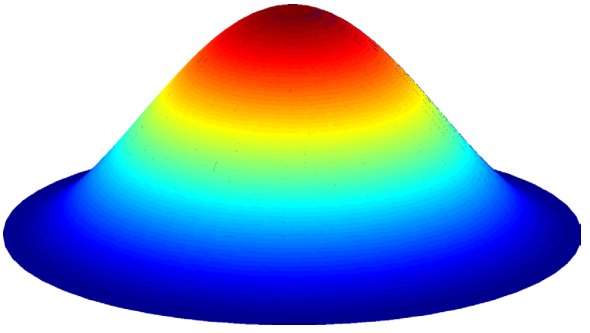

Fig. 31. Clamped circular plate: eigenmode corresponding to ω_{01}.

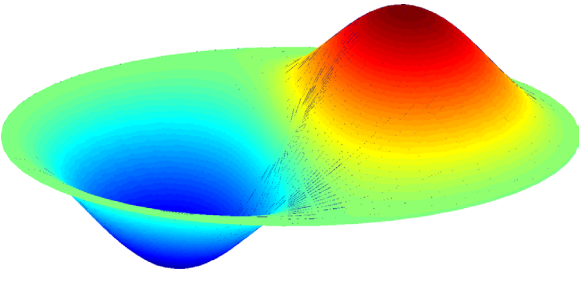

Fig. 32. Clamped circular plate: eigenmode corresponding to ω_{11}.

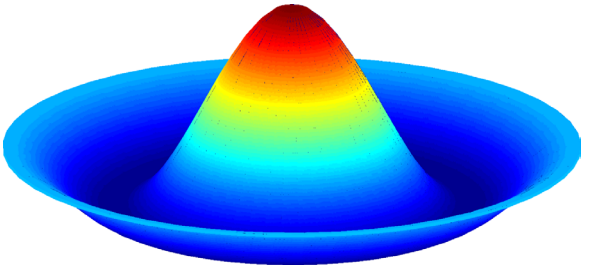

Fig. 33. Clamped circular plate: eigenmode corresponding to ω_{02}.

6. Conclusions

In the present work the recently introduced concept of Isogeometric Analysis [Hughes *et al.*, 2005] has been applied to the study of structural vibrations.

After a review of some basics of Non-Uniform Rational B-Splines and of Isogemetric Analysis main ideas, the determination of the structural frequencies for different problems has been presented.

In particular one-dimensional (like rods and beams) and two-dimensional problems (like membranes and plates) have been studied. The method has shown very

good results in all of these cases and has achieved a superior behaviour when compared with analogous classical finite element results. Another investigated issue has been the possibility of developing, in a natural way, one- and two-dimensional rotation-free thin bending elements. Imposition of boundary conditions on rotations both weakly and with Lagrange multipliers has been addressed for one-dimensional rotation-free elements.

Finally the exact geometry property of the method has been exploited in order to study a three-dimensional circular problem. In this example, the capability of the method of studying thin bending structures (a plate in this case) by means of 3D solid elements has been tested as well, obtaining again good results.

Since these preliminary results have shown that this technique could constitute an important tool in the framework of structural vibrations, more research in this context is going to be undertaken for the future. Interesting issues are studies on different parametrisations (in particular to avoid the appearance of what have been called "outlier frequencies") and on lumped mass formulations. Finally, the method needs to be deeply tested versus experimental results in different cases of geometrically complicated real structures, where it seems to be particularly effective, as shown by the studies on the NASA Aluminium Testbed Cylinder reported in Cottrell *et al.* [2005a,b].

Acknowledgments

The author would like to thank Professor T. J. R. Hughes for supporting and supervising him as a visiting scholar at the Institute for Computational Engineering and Sciences (University of Texas at Austin) where the research project reported herein has been carried out, as well as Professor Ferdinando Auricchio for his constant encouragement. This work has been partially supported by the European School for Advanced Studies in Reduction of Seismic Risk (Pavia) and by Servizio Sisimico Nazionale – Dipartimento della Protezione Civile (Roma).

References

Chopra, A. K. [2001] *Dynamics of Structures. Theory and Applications to Earthquake Engineering, Second Edition* (Prentice-Hall, Upper Saddle River, New Jersey).

Clough, R. W. and Penzien, J. [1993] *Dynamics of Structures* (McGraw-Hill, New York).

Cottrell, J. A., Hughes, T. J. R., Bazilevs, Y. and Reali, A. [2005a] "Isogeometric analysis: Exact geometry and accurate analysis of real structures," *Proceedings of the 8th US National Congress on Computational Mechanics*, Austin, Texas.

Cottrell, J. A., Reali, A., Bazilevs, Y. and Hughes, T. J. R. [2005b] "Isogeometric analysis of structural vibrations: k-refinement, invariant frequency spectra, nonlinear parametrization, rotationless bending elements, and application to an exact geometrical model of the NASA aluminium testbed cylinder," submitted to *Computer Methods in Applied Mechanics and Engineering*.

Engel, G., Garikipati, K., Hughes, T. J. R., Larson, M. G., Mazzei, L. and Taylor, R. L. [2002] "Continuous/discontinuous finite element approximations of fourth-order elliptic problems in structural and continuum mechanics with applications to thin beams and plates, and strain gradient elasticity," *Computer Methods in Applied Mechanics and Engineering* **191**, 669–3750.

Fried, I. and Malkus, D. S. [1976] "Finite element mass lumping by numerical integration without convergence rate loss," *International Journal of Solids and Structures* **11**, 461–466.

Hilber, H. M., Hughes, T. J. R. and Taylor, R. L. [1977] "Improved numerical dissipation for time integration algorithms in structural dynamics," *Earthquake Engineering and Structural Dynamics* **5**, 283–292.

Hughes, T. J. R. [2000] *The Finite Element Method: Linear Static and Dynamic Finite Element Analysis* (Dover Publications, Mineola, New York).

Hughes, T. J. R., Cottrell, J. A. and Bazilevs, Y. [2005] "Isogeometric analysis: CAD, finite elements, NURBS, exact geometry and mesh refinement," *Computer Methods in Applied Mechanics and Engineering*, **194**, 4135–4195.

Meirovitch, L. [1967] *Analytical Methods in Vibrations* (The MacMillan Company, New York).

Montgomery, D. C., Runger, C. and Hubele, N. F. [2003] *Engineering Statistics*, 3rd ed. (Wiley, New York).

Oñate, E. and Cervera, M. [1993] "Derivation of thin plate bending elements with one degree of freedom per node: A simple three node triangle," *Engineering Computations* **10**, 543–561.

Oñate, E. and Zarate, F. [2000] "Triangular plate and shell elements," *International Journal for Numerical Methods in Engineering* **47**, 557–603.

Phaal, R. and Calladine, C. R. [1992] "A simple class of finite-elements for plate and shell problems. 2. An element for thin shells with only translational degrees of freedom," *International Journal for Numerical Methods in Engineering* **35**, 979–996.

Piegl, L. and Tiller, W. [1997] *The NURBS Book*, 2nd Edition (Springer-Verlag, New York).

Prudhomme, S., Pascal, F., Oden, J. T. and Romkes, A. [2001] "A priori error estimate for the Baumann-Oden version of the discontinuous Galerkin method," *Comptes Rendus de l'Academie des Sciences I, Numerical Analysis* **332**, 851–856.

Reali, A. [2004] "An isogeometric analysis approach for the study of structural vibrations," M.Sc. Thesis, European School for Advanced Studies in Reduction of Seismic Risk, Università degli Studi di Pavia, Italy.

Rogers, D. F. [2001] *An Introduction to NURBS With Historical Perspective* (Academic Press, San Diego, CA).